A Communication Theoretical Modeling and Analysis of Underwater Magneto-Inductive Wireless Channels

Burhan Gulbahar and Ozgur B. Akan, *Senior Member, IEEE*

***Abstract*—Underwater physical medium is a challenging environment for communication using radio frequency (RF) or acoustic waves due to strong attenuation, delay, multi-path fading, power and cost limitations. Discovered a century ago, magneto-inductive (MI) communication technique stands as a strong alternative paradigm due to its independence of environmental impairments including multi-path fading, dynamic channels and high propagation delays experienced by acoustic waves. Furthermore, MI technique yields networking solutions exploiting low-cost, easily-deployable and flexible antenna structures, and the possibility of forming networks of magnetic waveguides defeating path loss. In this work, highly power efficient and fully connected underwater communication networks (UWCNs) composed of transceiver and relay induction coils are presented. Three dimensional (3D) UWCNs are analysed in terms of basic communication metrics, i.e, signal-to-noise ratio, bit-error rate, connectivity and communication bandwidth. The performance studies of realistic 3D networks covering hundreds of meters sea depths and a few km^2 areas show that fully connected multi-coil networks with communication bandwidths extending from a few to tens of KHz are possible. Furthermore, the performance dependence on coil properties and network size is theoretically modelled. Results show that MI wireless communication is a promising alternative for UWCNs and future research challenges are pointed out.**

***Index Terms*—Underwater magnetic wireless communications, magnetic-induction, induction coil, 3D grid network.**

I. Introduction

UNDERWATER communication is traditionally achieved by using acoustic [1], [2], radio frequency (RF) [2]–[5] and optical channels [6]. The major drawbacks of these channels prevent them from being fully reliable and practical technologies for underwater communication.

In underwater RF communication, electromagnetic waves propagate over very short distances due to high levels of attenuation [2], [4] increasing with conductivity and frequency. Large antenna size, low operation frequencies [5] and high transmission power [1] are necessary. Similar problems are also observed in underground channels which are similar to underwater channel conditions, e.g., salty water content and dynamically changing conditions [7].

Manuscript received October 31, 2011; revised March 21, 2012; accepted June 4, 2012. The associate editor coordinating the review of this paper and approving it for publication was J. Wu.

The authors are with the Next-generation and Wireless Communications Laboratory (NWCL), Department of Electrical and Electronics Engineering, Koc University, Istanbul, Turkey (e-mail: {bgulbahar, akan}@ku.edu.tr).

This work was supported by the Turkish National Academy of Sciences Distinguished Young Scientist Award Program (TUBA-GEBIP).

Digital Object Identifier 10.1109/TWC.2012.070912.111943

In underwater optical channels, the source and destination nodes should form a directional link in a close proximity [6] with high precision in pointing the narrow laser beams [1]. Furthermore, the multiple scattering of light results in dispersion and creates the intersymbol interference [8].

In underwater acoustic channels, which is the most promising technology used currently due to longer propagation distances underwater [4], there are several major difficulties such as frequency-dependent propagation loss, multipath fading, high propagation delay, limited bandwidth, temporary losses of connectivity, extreme Doppler and wideband effects [1], [9].

Another very promising low-cost, robust and efficient method is the magneto-inductive (MI) wireless communication [7], [10]. Unlike acoustic channel, MI channel does not have high latency [11], [12] and it mitigates the challenges of dynamical conditions and high power consumptions by using simple, low cost and low power coils [7]. The channel conditions depend on the permeability of the communication medium and a uniform channel is created in air, seawater and most types of soil and rock due to almost the same permeability. Furthermore, the feasible communication distance dramatically increases with waveguides [7], [10].

MI waveguides are introduced in [13] based on coupled and capacitively loaded loops with analysis by using a circuit model and considering both nearest and distant neighbor effects with potential applications like power dividers, bends and couplers for 1D, 2D and 3D in [14]. Similar applications like guiding RF energy and general N-port devices including power splitters and directional couplers are presented in [15] assuming lossless propagation and nearest neighbour coupling. Non-nearest neighbor interactions in MI waveguides are investigated in [16]. However, in none of these works, 3D MI wireless networks are considered with a communication theoretical modeling, performance analysis and application in underwater communication networks.

MI communication is recently introduced in wireless underground communication (WUC) networks [7], [10]. Underground MI channel is theoretically analyzed and compared with RF channels and MI waveguides are utilized. In [17], MI WUC in a district heating system is explored by analyzing a two-coil system in terms of antenna design. In [18], deployment of waveguides to connect sensors is analyzed by optimizing the number of coils and increasing the network robustness. Similarly, MI waveguides are explored in [19] in

terms of system architecture and operational framework to be used for underground pipeline monitoring. MI waveguides are extended by analyzing various array excitation schemes in [20]. However, these works are mainly concentrated on WUC networks, consider 1D topologies and nearest neighbor interactions. On the contrary, in this work, 3D MI wireless network topology is theoretically analyzed in terms of communication theoretical performance metrics by considering non-nearest neighbor interactions and realistic 3D grid underwater wireless networks are explored and numerically analyzed.

There is a limited number of work using MI communication in underwater. Early work is considered in [21] where a number of SNR and BER experiments are performed by Coastal Systems Station (CSS) and Magneto-Inductive Systems Limited (MISL). Two-coil links using AC magnetic fields are experimented with modulation schemes like PSK, FSK and MSK. About tens of bits/s data rate is achieved in seawater at a couple of KHz operating frequency and at ranges of hundreds of meters. On the other hand, this work does not provide the theoretical modeling and the topology design considering multiple coils. Besides that, in patent files in [22], [23], two-way submarine communication systems composed of submerged coil unit at the basement of the water and a remote station outside of the water are introduced. A similar one in [24] explains an MI relay system and their application areas as sensors in various areas including underwater. In [25], data link and physical link layer protocol stack is presented for magnetic area communication networks to be used in various mediums such as rock, soil and water. However, underwater MI wireless communication networks are not considered, theoretical and performance analyses are not given.

Near-field magnetic communication (NFMC) studies explore induction in two-coil close distance communication systems. In [11], the bubble like coverage of short-range magnetic communication system is analyzed. Similarly, in [12], NFMC is used with low power quasi-static magnetic fields operating at frequency 13.56 MHz. In [26], a two-coil system is analyzed in terms of link capacity, range and coil properties. In [27], 3-dB bandwidths of solenoidal loop antennas are theoretically analyzed by using equivalent circuits. However, these works do not discuss 3D theoretical modeling of coil networks and communication theoretical performance metrics.

Another application area of MI technique is wireless power transfer. In [28], an efficient system using inductive coils is presented and a similar system is described in [29] by providing communication protocol. Near-field power transfer is analyzed theoretically and experimentally by using multiple transmitters [30] and by using multiple receivers [31]. However, these works are missing in terms of 3D theoretical modeling of the coil networks considering their full mutual inductance calculations and inter-coil effects, and communication theoretical performance metrics are not analyzed.

In this work, 3D underwater MI wireless networking topologies formed with circular coils oriented with three degrees of freedom are, for the first time, theoretically modeled in terms of power loss and signal-to-noise ratio (SNR) by considering non-nearest neighbor interactions. The derived model is, for the first time, applied to 3D grid networks designed for practical shallow and deep water, and for long range or large area underwater networks. SNR, bit-error rate (BER), connectivity and bandwidth performance metrics are analyzed for various underwater MI wireless networks with binary phase shift keying (BPSK) modulation. Relaying coils without power consumption form a power-efficient networking. It is shown that high SNR communication bandwidths extending from a few to tens of KHz are possible for small coverage areas in shallow water and a few km^2 large areas in deep water, respectively, by using a couple of meter radius coils forming a fully connected and power efficient multi-coil network. Furthermore, the detailed theoretical analysis of the performance depending on coil parameters and grid size is presented.

The remainder of this paper is organized as follows. In Section II, two-coil MI communication channel in a 3D underwater environment is theoretically modeled and power loss for two-coil and general multi-coil network topologies are theoretically analyzed. After deriving the communication models, in Section III, 3D grid networks are presented for underwater and SNR, BER, connectivity and bandwidth performances are numerically analyzed. Then, the performance dependence of the grid network on coil parameters and grid size is analyzed. Finally, In Section IV, conclusions are given and future works are pointed out.

II. Underwater Magnetic Induction Communication Networks

In this section, firstly, MI underwater channel is discussed. Next, the basic two-coil channel in a 3D environment is modeled by using the general mutual inductance calculations and equivalent circuit methods. Then, for a general multi-coil 3D topology, the power loss performance is theoretically modeled by fully exploiting the inter-coil mutual inductance relationships. Then, the resulting analysis is simplified by using Thevenin equivalent circuit description.

A. Underwater magnetic induction channel

Induction coil sensors are one of the oldest types of magnetic sensors [32]. When two n_t-turn inductor coils exist together, a flux created by one coil linking the other induces a voltage. Any two coils with an enough mutual inductance relation can transfer power by MI channel.

In underwater, coils have dynamic positions, orientations and distributions making simplifying assumptions necessary. Nodes are assumed static and the analysis of velocity or dynamic effects is planned for future work. Furthermore, the small movements compared with inter-coil distance do not lead to significant differences in mutual inductances. In this article, the formulation of the general problem is emphasized with models depending on the distance, coil sizes, static topology etc. forming the background for future analyses. Furthermore, permeability of the air and water are taken as the same [10], i.e., $\mu_0 = 4\,\pi\,10^{-7}$ H/m. Therefore, MI channel creates a homogeneous medium between underwater-underwater and underwater-surface areas. The coils are assumed to have three degrees of freedom in terms of central (c) and axis (d) distances, and the angular misalignment θ between the axes of the coils as shown in Fig. 1 [33]. In

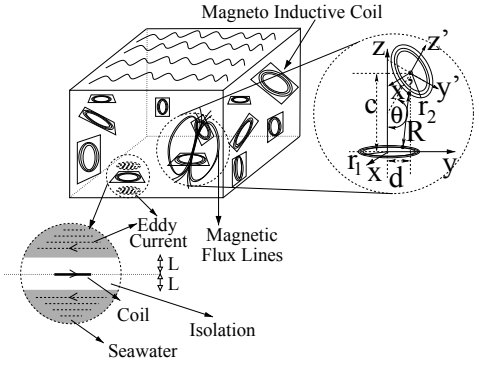

Fig. 1. Underwater network of coils, detailed orientation of two coils w.r.t. each other with three degrees of freedom, and the model for eddy currents.

this article, circular coils are analyzed to simplify the mutual inductance analysis. However, in literature, various antennas, e.g., combining circular coils in orthogonal axes, are used for position and orientation tracking [34]. Their usage in underwater is out of scope as a subject of future work. Series capacitor is attached to the transceivers to achieve flexibility in operating characteristics.

The eddy currents can be important in seawater due to finite amount of conductivity, i.e., $\sigma = 4$ S/m [35] and for a circular coil surrounded by finite depth isolating layers, e.g., free space, they are analyzed by using the simplified modeling in [36] by assuming that they are minimized by placing the coils in an isolated box as shown in Fig. 1 where the distance between the coil plane and the seawater is L_d (m). The current largely concentrates in circular rings extending to the depth of $\delta = \sqrt{1 / (\pi \mu_0 f \sigma)}$, i.e., skin depth. For seawater, δ is ≈ 10 cm for operation frequency of $f \approx 5$ MHz, ≈ 25 cm for $f \approx 1$ MHz and ≈ 8 m for $f \approx 1$ KHz. In this article, for $f \approx 5$ MHz, a very small depth of water includes the eddy current by assuming it lowers the current in the transmitter coil for its effect on coils of tens of meters apart. The modeling in [36] assuming an isolation layer with infinite length and finite depth is used to approximate the opposing circular eddy current amount between radius $r_{e,1}$ and $r_{e,2}$ as

$$\vec{J}_{eddy} = -\vec{\phi}\, j\, 2\pi f \sigma \int_0^{\infty} \int_{r_{e,1}}^{r_{e,2}} A_{\phi}(r_e, z)\, \mathrm{d}r_e\, \mathrm{d}z \quad (1)$$

where $A_{\phi}(r_e, z)\vec{\phi} = \vec{\phi} \int_0^{\infty} C\, e^{-\alpha_1 (z+L_d)}\, J_B(\alpha r_e)\, \mathrm{d}\alpha$ is the vector potential at the radius r_e and vertical position z inside the water as shown in Fig. 1, C is a constant which can be found by using the continuity of electric and magnetic fields at boundaries, $J_B(.)$ is Bessel function of the first kind and order one, $\alpha_1 = \sqrt{\alpha^2 + j\, 2\pi \mu_0 \sigma}$, $\vec{\phi}$ is the unit angular vector. Therefore, in the following, L_d is chosen large enough to neglect $\vec{J}_{eddy}$. Next, self and mutual inductance calculations are achieved for two-coil systems in 3D.

B. Two-coil mutual inductance analysis

Underwater coils are open to disturbances resulting from water currents and wave effects making it necessary to analyze the mutual inductance relations among coils by considering the problem in 3D. The mutual inductance between two circular coils having 3D positional freedom with both lateral and angular misalignments is found in [33] by using the magnetic flux Φ flowing through one of the coils and using the Stokes's theorem to find the magnetic flux by using the magnetic vector potential through the respective coil. The mutual inductance M among two coils of radius r_1 and r_2 is described as $M = \Phi / I_1$ where Φ is the magnetic flux flowing through second coil due to first coil carrying current I_1. Φ is expressed as $\Phi = \int_S \boldsymbol{\nabla} \times \vec{\mathbf{A}}\, \mathrm{d}\mathbf{s} = \oint_{C_2} \vec{\mathbf{A}}\, \mathrm{d}\ell$ where $\vec{\mathbf{A}}$ is the magnetic vector potential of the first coil on the area of the second coil, S is the corresponding area of the second coil, $\boldsymbol{\nabla}\times$ is the curl and C_2 is closed path curve along it [37]. $\vec{\mathbf{A}}$ is found as $\vec{\mathbf{A}} = (\mu_w / (4\pi)) \int_{C_1} (I_1 / p)\, \mathrm{d}\ell'$ where p is the distance from a point on the first coil closed path to the point on the second coil path as shown in Fig. 1 and μ_w is the magnetic permeability of the underwater medium. Magnetic permeability of the water, air and the salt are almost the same [10] where μ_0 is used in the computations.

Algebraic manipulations lead to the following [33],

$$M = \left(n_t^2\, 2\mu_0 \sqrt{r_1 r_2} / \pi\right) \times \int_0^{\pi} \left(\cos(\theta) - d\, \cos(\phi) / r_2\right) \Psi(k) / \left(k \sqrt{\zeta^3}\right) \mathrm{d}\phi \quad (2)$$

where $\Psi(k) = (1 - k^2/2)\, K(k) - E(k)$, $\zeta = \sqrt{1 + d^2 / r_2^2 - \eta}$, $k^2 = 4\chi\zeta / ((1+\chi\zeta)^2 + \delta^2)$, $\eta = \sin^2(\theta)\, \cos^2(\phi) + 2\, d\, \cos(\theta)\, \cos(\phi) / r_2$, $\chi = r_2 / r_1$, $\delta = \kappa - \chi\, \cos(\phi)\, \sin(\theta)$, $\kappa = c / r_1$, $K(k) = \int_0^{\pi} \left(1 / \sqrt{1 - k^2\, \sin^2(\theta)}\right) \mathrm{d}\theta$ and $E(k) = \int_0^{\pi} \sqrt{1 - k^2\, \sin^2(\theta)}\, \mathrm{d}\theta$ are elliptic integrals, r_1 and r_2 are the radii of two coils as shown in Fig. 1.

Self inductance, i.e., L, and resistance, i.e., R, of a circular coil are computed as $L = 0.5\, \mu_0\, \pi\, n_t^2\, r$ and $R = 2\, \pi\, n_t\, r\, R_0$ where R_0 is resistance per meter depending on the type of the wire and its diameter. Next, the presented calculations are used in an equivalent circuit model to analyze power loss in the MI link to be later used in SNR calculations.

C. Equivalent circuit analysis

Two-coil and multi-coil equivalent circuit representations are derived modeling the power transferred from the transmitter to receiver. The derived models can be used to compute SNR dependence on transmit power and network topology. Circular coils are modeled as circuits linked with a mutual inductance. Firstly, simply coupled two coils are analyzed.

1) Two-coil equivalent circuit analysis: MI link is formed by the induction among primary and secondary coils resulting from the alternating current of the primary coil. The radius r, the number of windings n_t and the series capacitance C affect the link properties. Since L and R are variables of r and n_t, the nodes have the same inductance and resistance. The conventional *RLC* circuit representations can be used to analyze the power transfer characteristics among coils since the working principle of MI communication system depends on the induced current. MI link and its equivalent circuit representation are shown in Fig. 2 where Z_r and Z_t are the total intrinsic impedances of the receiving and the transmitter sides, Z_r^{refl} and Z_t^{refl} are the reflected impedances on the

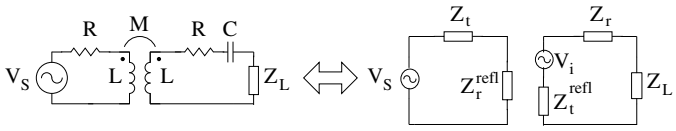

Fig. 2. Basic transformer circuit with MI link achieved by mutual induction M and equivalent circuit representation.

transmitter and receiver sides, respectively, V_s is the voltage source, V_i is the induced voltage on the secondary coil and Z_L is the load impedance. After equivalent circuit analysis, impedance values are found as $Z_r = 1\,/\,(\jmath\omega\,C) + R + \jmath\omega\,L$, $Z_t = Z_r$, $Z_r^{refl} = \omega^2\,M^2\,/\,(Z_r + Z_L)$ and $Z_t^{refl} = \omega^2\,M^2\,/\,Z_r$ where $\omega = 2\,\pi\,f$ and f is the operating frequency. V_i becomes $(-\jmath\omega M\,/\,Z_r)\;V_s$. The transmitted power P_t is the power consumed in the first loop of the equivalent circuit and the received power P_r is the consumed one in Z_L. After some algebraic manipulations, the following is found for their ratio, i.e., $P_r\,/\,P_t = \mathrm{Re}\{Z_L\,|V_i|^2\,/\,\left|Z_t^{refl} + Z_L + Z_r\right|^2\}\,/\,\mathrm{Re}\{|V_s|^2\,/\,\left(Z_t + Z_r^{refl}\right)^*\}$ where Re denotes the real part. To operate at the maximum power efficiency, Z_L should be matched to the receiver side, i.e., $Z_L = \left(Z_r + Z_t^{refl}\right)^*$, at a specific frequency $\omega_0 = 2\,\pi\,f_0$ leading to $Z_L = \omega_0^2\,M^2\,/\,(R - \jmath\omega_0\,L)$ + $R - 1\,/\,(\jmath\omega_0\,C) - \jmath\omega_0\,L$. Then, $P_r\,/\,P_t = 0.5\left(1 + 2R^2\,/\,(\omega_0^2\,M^2)\right)^{-1}$ is found at ω_0.

Due to the high attenuation of MI waves, waveguides are formed by using passive relay coils enlarging the traveling distance of waves [7], [10]. In [7], [10], by using the nearest neighbor approximation between adjacent coils and adjusting the capacitance values, an improvement is obtained. In this paper, the effects of relay coils in 3D underwater ad hoc topologies are explored in a theoretical model considering non-nearest neighbor interactions [14], [16]. Next, a multi-coil case is considered and the resulting power transfer ratio is derived.

2) Multi-coil equivalent circuit analysis: In a 3D topology, one of the coils serve as the transmitter, one as the receiver with active Z_L, and the others behave as passive relay coils with no power consumption. The coils are assumed to be interchangeably acting either as transmitter, receiver and the relay. Thus, passive relays lead to a power efficient networking different from the classical relaying mechanism consuming power. In the following, general formulation of the problem permits extension to include multiple sources or receivers in multiple access (MAC), broadcast or multiple-input and multiple-output (MIMO) frameworks including the crosstalk analysis. In this work, all relays are used by only one active communication link between a single transmitter and a receiver. Crosstalk analysis in multi-transmitter and multi-receiver is a subject of future work.

Using Kirchoff's Law and considering non-neighbor relations, the equations combining voltage sources ($\mathbf{V}$) and coil currents ($\mathbf{I}$) can be written in matrix form as [14], [16]

$$\mathbf{M}\,\mathbf{I} = \mathbf{V};\;\mathbf{I} = [I_1\;I_2\;\ldots I_n]^T;\;\mathbf{V} = [V_s\;0\;\ldots 0]^T \qquad (3)$$

where $()^T$ denotes transpose, $\mathbf{M}$ is $n \times n$ matrix with elements $\mathbf{M}(i,j) = \jmath\omega\,M_{i,j}$ for $i \neq j$, Z_i for $i = j \leq n-1$ and $Z_n + Z_L$ for $i = j = n$, $Z_i = R_i + j\omega L_i + 1\,/\,(j\omega C_i)$, $M_{ij} = M_{ji}$ and n is the total number of coils and denotes the index of the receiver coil. Assuming that $\mathbf{M}$ has an inverse $\mathbf{M}^{-1}$, current vector $\mathbf{I}$ becomes $\mathbf{I} = \mathbf{M}^{-1}\,\mathbf{V}$. Then, the transmitted and received power are expressed as $P_t = 0.5\,\mathrm{Re}\{\mathbf{V}^H\mathbf{I}\}$ and $P_r = 0.5\,|I_n|^2\,\mathrm{Re}\{\mathbf{Z}_L\}$, respectively, leading to the expression valid for all topologies where $()^H$ denotes Hermitian.

Furthermore, an alternative representation simplifies the calculation for large number of coils with symmetric geometry by using Thevenin equivalent voltage and impedance for the receiver. Let us define $k \times k$ matrix $\mathbf{M}_{k,k}^{\omega}$ with elements $\mathbf{M}(i,j) = \jmath\omega\,M_{i,j}$ for $i \neq j$ and Z_i for $i = j$, and the vectors $\mathbf{M}_{n,1} = [M_{n,1}\;M_{n,2}\;\ldots M_{n,n-1}]^T$, $\mathbf{I}_{n,1}^{oc} = \left[I_1^{oc}\;I_2^{oc}\;\ldots\;I_{n-1}^{oc}\right]$ and $\mathbf{V}_{n-1} = [V_s\;0\;\ldots\;0]$ where I_j^{oc} denotes current in coil number j when the n'th coil is open circuited. Furthermore, assume that Z_L is matched to ω_0. Moreover, whenever the inverse of $\mathbf{M}_{k,k}^{\omega}$ is available, denote it by $\Gamma_{k,k}^{\omega} = (\mathbf{M}_{k,k}^{\omega})^{-1}$. Then, open circuit voltage V_{oc} at the n'th coil and the Thevenin equivalent impedance Z_{Th}^{w} seen by n'th coil are represented by $V_{oc} = \jmath\omega\,\mathbf{M}_{n,1}^T\Gamma_{n-1,n-1}^{\omega}\mathbf{V}_{n-1}$ and $Z_{Th}^{\omega} = (\Gamma_{n,n}^{\omega}(n,n))^{-1} = \det|\mathbf{M}_{n,n}^{\omega}|\,/\,\det|\mathbf{M}_{n-1,n-1}^{\omega}|$ where $\Gamma_{n,n}^{\omega}(i,j)$ denotes the i,j'th element of the matrix and $\det|\mathbf{M}|$ denotes the determinant of a matrix $\mathbf{M}$. Then, the matched impedance load $Z_L^{\omega_0}$ is found by taking the complex conjugate of $Z_{Th}^{\omega_0}$. Then, P_r is found as follows,

$$P_r = 0.5\,\mathrm{Re}\{Z_{Th}^{\omega_0}\}|V_{oc}|^2\,/\,|Z_{Th}^{\omega} + (Z_{Th}^{\omega_0})^*|^2 \qquad (4)$$

Similar Thevenin circuit analysis for the source is achieved by using $\mathbf{M}_a^{\omega}$ with elements $\mathbf{M}_a^{\omega}(i,j) = \mathbf{M}_{n,n}^{\omega}(i,j)$ for $(i,j) \neq (n,n)$ and $\mathbf{M}_{n,n}^{\omega}(n,n) + Z_L^{\omega_0}$ for $i = j = n$, and $(n-1) \times (n-1)$ matrix $\mathbf{M}_b^{\omega}$ with elements $\mathbf{M}_b^{\omega}(i,j) = \jmath\omega\,M_{i+1,j+1}$ for $i \neq j$, Z_{i+1} for $i = j \leq n-2$ and $Z_n + Z_L^{\omega_0}$ for $i = j = n-1$. Defining $\Gamma_a^{\omega} = (\mathbf{M}_a^{\omega})^{-1}$, Thevenin equivalent impedance for the source coil and P_t can be found as follows,

$$\begin{aligned} Z_{Th}^{coil1} &= (\Gamma_a^{\omega}(1,1))^{-1} = \det|\mathbf{M}_a^{\omega}|\,/\,\det|\mathbf{M}_b^{\omega}| \\ &= \left(\det|\mathbf{M}_{n,n}^{\omega}| + Z_L^{\omega_0}\det|\mathbf{M}_{n-1,n-1}^{\omega}|\right)\,/\,\det|\mathbf{M}_b^{\omega}| \qquad (5) \end{aligned}$$

$$\begin{aligned} P_t &= 0.5\,|V_s|^2\mathrm{Re}\{1/(Z_{Th}^{coil1})^*\} = 0.5\,|V_s|^2 \\ &\times \mathrm{Re}\{(\det|\mathbf{M}_b^{\omega}|)^*/(\det|\mathbf{M}_{n,n}^{\omega}| + Z_L^{\omega_0}\det|\mathbf{M}_{n-1,n-1}^{\omega}|)^*\} \qquad (6) \end{aligned}$$

These equations are used to simplify the power transfer ratio instead of taking the resource consuming operation of taking inverse of mutual inductance matrix. Next, the grid networks for underwater are introduced and their communication theoretical performance analysis is given.

III. MI Underwater Wireless Network Performance Analysis

In this section, numerical and theoretical performance analyses of 3D grid underwater MI wireless networks are achieved. SNR, BER, connectivity and bandwidth performances are simulated for the networks extending along a line, e.g., sea shore, in shallow water and having rectangular area coverage in deep water. Then, performance dependence on coil radius, wire diameter, capacitance and inter-coil distance is analyzed for grids of variable sizes and volumes.

3D grid network topology is seen in Fig. 3. The distances between coils in 2D layers parallel to the sea surface (x-y)

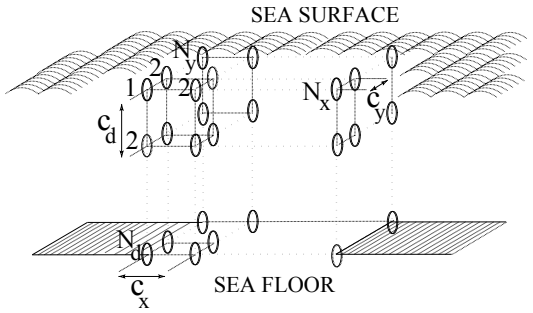

Fig. 3. 3D grid topology for shallow and deep water networking coverage.

TABLE I
COIL AND SIMULATION PARAMETERS FOR GRID NETWORK

Parameter	Meaning	Value
r_w	The copper wire radius	0.725 mm
r	The coil radius	5 m
n_t	The number of windings	3
W	Weight of the copper coil	$\simeq 1.38$ kg
C	The capacitance of coil unit	10 pF
L	The inductance of coil unit	$\approx 89\,\mu$H
R_0	Unit resistance of the wire	$\approx 0.01\,\Omega$/m
R	The resistance of coil unit	$\approx 1\,\Omega$
f_0	Operating frequency	≈ 5.34 MHz
P_n	Noise Power	$-120,\ -75,\ -30$ dBm

are denoted by c_x and c_y and the distance along the depth is denoted by c_d. The coils form a $n = N_x \times N_y \times N_d$ size grid network in a volume $V = (N_x - 1)(N_y - 1)(N_d - 1)\, c_x\, c_y\, c_d$ of water. The variables can be adapted depending on requirements such as performing in deep or shallow water, small or large area coverage. The coils weighting a few kgs can be hold in their positions by floating buoys for a dynamic network [1].

Some realistic assumptions are made for coil properties, e.g., having the same number of windings, resistance, inductance and series capacitance. The network is assumed to be designed at ω_0 chosen as the resonance frequency of the basic RLC structure of each coil, i.e., $\omega_0 = 1/\sqrt{L\,C}$ [7], [10]. However, for small inter-coil distances of grid networks, it is observed that the frequency giving the maximum power transfer shifts from the designed ω_0 such that a frequency search is applied. R_0 depends on specific resistance of the wire, i.e., copper wire with $\rho = 1.72\,10^{-8}\,\Omega\,$m and the wire diameter r_w such that $R_0 = \rho/\pi\, r_w^2$. In this article, coils with American wire gauge (AWG) size 15, 17 and 20 (radius between 0.4060 to 0.7250 mm) are used. The weight of the copper coil is computed by $W = 8.9\,10^3\,(\pi\, r_w^2)\,(2\pi\, r\, n_t)$ where the density of the copper wire is $8.9\,10^3\,\mathrm{kg/m^3}$. The precautions mentioned in [7] should be cared such that the capacitance should be larger than 10 pF and f_0 should be lower than 10 MHz to reduce the parasitic capacitance.

In the first experiment, the performance is analyzed with fixed coil parameters given in Table-I. In the second one, the wire radius in 0.4060 to 0.7250 mm, capacitance in 10-50 pF and radius between 1-30 m are simulated for analysis of performance dependence on coil parameters.

Eddy current by using (1) is calculated for $0 \le L_d \le 4$ m for rings at r_e with width $r_{e,2} - r_{e,1}$ of either 5 cm or 1 m such that the currents for 5 cm wide rings represent local currents and 1 m wide rings represent the cumulative eddy current. It is observed that the current density becomes maximum for $r_e = r$. The real part of eddy current in 5 cm and 1 m wide rings at $r_e = r = 5$ m (simulated size of the coils) becomes $\approx \%10$ and $\approx \%50$ of the current in the coil, respectively, for no isolation layer, i.e., $L_d = 0$. These values are large enough making isolation necessary. With $L_d = 4$ m, the values become $\approx \%0.25$ and $\approx \%5$ which can be further decreased by increasing L_d. As a result, in simulations, it is assumed that eddy current is minimized and neglected.

P_n is assumed to be in the range $(-120,\ -30)$ dBm simulating much higher noise levels compared with the literature, i.e., -83 dBm [7], and with thermal noise power (P_t) being in the interval $\approx (-130,\ -115)$ dBm calculated in simulations for the parameters specified in Table-I and grid network topologies. P_t is computed by $P_t = 4\,\kappa_B\,T\,B_r\,R_L\,/\,(R + R_L)$ where $\kappa_B = 1.38 \times 10^{-23}$ J/K is the Boltzmann constant, $T = 300$ K is the absolute temperature, B_r is the bit rate (in Kbit/s) and R_L is the load resistance [26], [38]. BPSK modulation is used leading to $BER = Q(\sqrt{2\,\mathrm{SNR}})$ where $Q(x) = 0.5\,\mathrm{erfc}(x/\sqrt{2})$ and $\mathrm{erfc}(x) = (2/\sqrt{\pi})\int_x^\infty e^{-x^2}\,\mathrm{d}x$ is the complementary error function [39].

In connectivity analysis, the term k-connectivity denotes a network that each node connects to k nodes within the specific BER threshold. A fully connected network means that all the nodes can connect to each other within the BER threshold. Next, the realistic network topologies are used to analyze the SNR, BER, connectivity and bandwidth performance.

A. SNR, BER, Connectivity and Bandwidth Performance

Two types of coverage topology are analyzed. Firstly, a rectangular prism with long range in x direction, e.g., along the shore of the sea, in shallow water is analyzed. $N_d = 2$, $N_y = 3$ and $c_d = c_y = 35$ m are chosen leading to a depth and width coverages of 35 m and 70 m, respectively. The total length of network is set to 400 m with variable N_x between 2-12 leading to varying c_x in $\approx$ 35-200 m. Each of $N_y \times N_d = 6$ coils at specific x axis position forms a 2D layer. The performance is analyzed in terms of inter-layer distance, i.e., L_x, for the effect of the number of layers by numerical simulation and comparison with single coil scheme composed of one transmitter and receiver without any relays. Secondly, $4 \times 4 \times 4$ grid network extending from 60 to 540 m depth with coverage area from 0.01 to $2\,\mathrm{km}^2$ is analyzed.

Various transmitter and noise power levels are simulated. For $P_t = 1$ dBm and $P_n = -60$ dBm, SNR performance of $N_x = 12$ layers grid network and its comparison with the single coil case are shown for nodes with varying inter-layer distance (x axis) in Fig.4(a). Maximum and minimum SNRs among the nodes having the specified x axis distance are compared. Single coil case simulation is performed by using only two coils at the respective positions of the grid network by removing all other coils except the transmitter and the receiver. It is observed that using only 2 coils shows significantly deteriorating performance dropping to 10 dB for the most distant position, e.g., $L_x = 400$ m. However, in the grid network, the most distant nodes communicate with SNR ≈ 50 dB and SNR is preserved almost constant along the

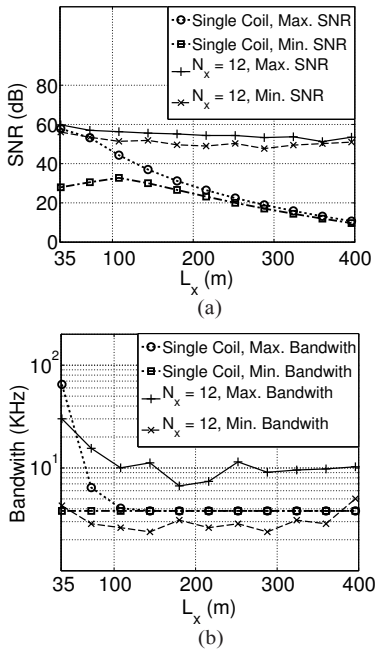

Fig. 4. Performances of $N_x = 12$ layer grid network and single coil scheme (no relay) for varying inter-layer distance (x axis) among the transmitter and the receiver nodes for (a) SNR and (b) bandwidth.

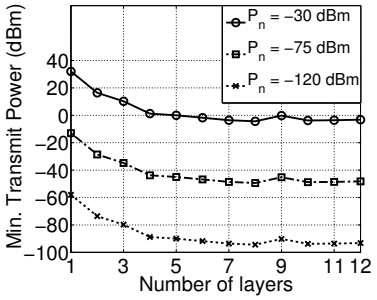

Fig. 5. The minimum required transmit power to form a fully connected grid network vs. varying number of layers (N_x) for varying noise power.

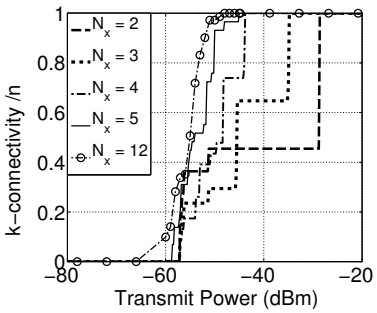

Fig. 6. k-connectivity of the network vs. P_t for varying number of layers.

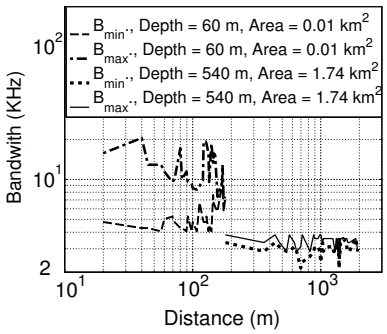

Fig. 7. Maximum and minimum communication bandwidth vs. the distance between transmitter and receiver coils for networks with varying physical size.

network. Therefore, similar to waveguides [7], grid network not only prevents SNR decay but also creates a connected network occupying a large 3D volume.

In Fig. 4(b), 3 dB bandwidth of the links between nodes having varying L_x is shown. It is observed that MI grid network has links with distance dependent bandwidth decreasing and saturating with the distance. Single coil case and grid network have around ≈ 60 and 30 KHz bandwidths among the nodes with layer distance $L_x \approx 36$ m, respectively. As the distance increases, single coil case allows ≈ 4 KHz communication while the grid network allows a much better ≈ 10 KHz bandwidth showing the advantage of forming MI networks.

The minimum required transmit power to form a fully connected grid network is shown for varying N_x and noise power in Fig. 5 for BER threshold of 10^{-6} which is enough for Kbit/s communication. As N_x increases, a more dense network is formed whereas the total volume is constant, i.e., $(N_x - 1) \times c_x = 400$ m. N_x indexed with 1 denotes the single coil case. As the noise power increases, the required power increases proportionally. Increasing the number of layers from 1 to 12 brings an improvement of ≈ 40 dBm transmit power required to form a fully connected network. The significant improvement obtained with relays not consuming any power results in a highly power efficient fully connected network. Furthermore, any coil which is not in transmitter mode behaves as passive relay coils to increase the power efficiency.

Connectivity of the network is shown in Fig. 6 for $P_n = -75$ dBm as P_t is increased. k-connectivity is divided by n to observe the respective coverage ratio. As the number of layers increases and the network gets dense, not only the required P_t is decreased but also P_t interval for the network transition from the fully disconnected state to fully connected state, i.e., (P_{fdisc}, P_{fconn}), gets lower. For $N_x = 12$, $P_{fdisc} - P_{fconn}$ is around 10 dBm whereas for $N_x = 2$ about 30 dBm. Therefore, both the power efficiency and the connectivity performance significantly increase with more dense passive relays.

In the second experimental analysis, $4 \times 4 \times 4$ network is analyzed for deep water. $c_x = c_y$ and c_d are chosen between 40-440 m and 20-180 m, respectively. The distance dependent bandwidths, i.e., min-max bandwidths (B_{min}, B_{max}) between coils, are observed in Fig. 7. The most dense topology permits 10 to 20 KHz bandwidth whereas the network covering a 540 m depth and 1.74km^2 area permits ≈ 4 KHz. M between coils is not spherically uniform and when combined with the interrelations in solution of (3) in a grid network, the observed bandwidth fluctuations occur as shown in Figs. 4(b) and 7.

BER of the worst performance link for varying P_t and physical size of the network is shown in Fig. 8 where $P_n = -75$ dBm. It is observed that the performance is highly dependent

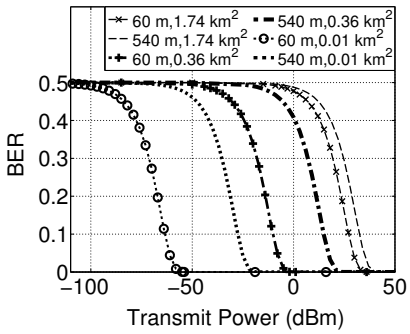

Fig. 8. BER of the worst link in the network vs. transmit power for networks with varying physical size.

on coverage area such that as the area increases, the effect of depth is reduced and the BER curves for various depths get closer. As the network size changes from 60 m depth, $0.01\,\mathrm{km}^2$ area to 540 m depth, $1.74\,\mathrm{km}^2$ area, the required power for low BER changes from ≈ -50 dBm to ≈ 40 dBm showing the high dependence of BER on inter-coil distance.

Comparing with other underwater wireless communication methods, i.e., acoustic, optical and RF, it permits long-range communication as a promising alternative to acoustic communication. The comparison of required power, transmission range, propagation speed and bit per joule (B/E) is shown in Table-II for state of the art underwater wireless communication technologies where the values for MI are approximated. Although coil size can be adjusted to the range of interest for MI waves and the relaying topology changes the performance significantly, the results given for 5 m radius coil and grid topology form a practical and comparable MI communication channel permitting several kms range of communication within tens of Kbit/s similar to acoustic channel but without high latency and propagation delay, multi-path fading, Doppler effects and large transceiver costs. Furthermore, for short range, although tens of Kbit/s data rate is very small compared with optical communication, it has a significantly large B/E ratio as shown in Table-II making it a promising low power alternative. Moreover, it has higher data rate compared with RF for the ranges extending from tens to hundreds of meters. Next, the dependence of performance on coil parameters and the grid inter-coil distance is analyzed.

B. Performance Dependence on Coil Parameters & Grid Size

In this section, a detailed theoretical analysis of the dependence of the power loss on coil radius, wire diameter, capacitance and the grid inter-coil distance is presented. Furthermore, an approximation is given for the power loss between transmitter and receiver by clarifying the proportionality of the performance dependence on coil parameters. $N \times N \times N$ cubic grid networks with uniform inter-coil distance, i.e., $l = c_x = c_y = c_d$, are analyzed for $N = 3$, 4 and 5 as practical real world scenarios. The maximum distance coils, i.e., at the opposite corners of the cube, are chosen as the transmitter and receiver. Firstly, the power loss between them is simulated for varying radius coils and varying l. The performance for $N = 4$ is seen in Fig. 9 observing that the

TABLE II
COMPARISON OF UNDERWATER WIRELESS COMMUNICATION CHANNELS

Type	Range (m)	Bandwidth (Kbit/s)	Power (W)	B/E (bits/J)	Speed (m/s)
Acoustic [41]	350	17.8	2	≈ 8900	≈ 1500
	1000	35.7	6	≈ 6000	
	10000	5	40	≈ 125	
Optical [42], [43]	2-48	10^6	-	-	$2.2\text{-}3\,10^8$
	40	10^4	36	≈ 280000	
	100	10^3	-	30000	
RF [44], [45]	0.2	10^4-10^5	-	-	$3\,10^8$
	10	156	15.84	≈ 9850	
	50	1-10	-	-	
	200	0.05-0.1	-	-	
MI	20-80	4-20	-	-	$3\,10^8$
	180	6-10	10^{-8}	$4\,10^8$-$2\,10^9$	
	200-600	3-4	-	-	
	2000	2-4	10	300-400	

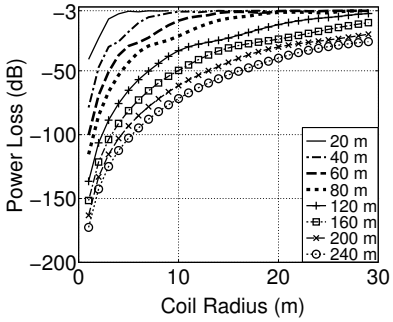

Fig. 9. The power loss between transmitter and the receiver vs. coil radius for varying inter-coil distance in $4 \times 4 \times 4$ grid network.

power loss saturates at -3 dB (same for $N = 3$ and 5) as the radius is increased for any l. Therefore, increase in the radius is unnecessary after saturation. To observe the dependence on coil parameters in a more detailed manner, a theoretical analysis can be given by using (4) and (5) to find the power loss. Algebraic manipulations at ω_0 lead to

$$P_r \,/\, P_t = 0.5 \left| \sum_{i=1}^{n-1} \jmath\,\omega_0\, M_{n,i}\, \Gamma^{\omega_0}_{n-1,n-1}(i,1) \right|^2 \times \left(\mathrm{Re}\{\det|\mathbf{M}_b^{\omega_0}| \,/\, \det|\mathbf{M}^{\omega_0}_{n-1,n-1}|\} \right)^{-1} \quad (7)$$

Let us define $(n-2)\times(n-2)$ mutual inductance matrix $\mathbf{M}_r^\omega$ for relays where $\mathbf{M}_r^\omega(i,j) = \jmath\,\omega\, M_{i+1,j+1}$ for $i \neq j$ and Z_{i+1} for $i = j$. Since $Z_i = R$ for $i \in (1, ..., n)$, $\mathbf{M}_r^\omega = R\,\mathbf{I}_\mathrm{U} + \jmath\,\omega\,\mathbf{M}^\omega_{offd}$ is obtained where $\mathbf{I}_\mathrm{U}$ is the identity matrix of size $n-2$ and $\mathbf{M}^\omega_{offd}$ is a $(n-2)\times(n-2)$ real symmetric matrix with elements $\mathbf{M}^\omega_{offd}(i,j) = M_{i+1,j+1}$ for $i \neq j$ and 0 for $i = j$. Since $\mathbf{M}^\omega_{offd}$ is real-symmetric, its eigenvalues are real and eigenvectors form a real orthogonal matrix (unitary) [40] letting it to be represented as $\mathbf{M}^\omega_{offd} = \mathbf{Q}\,\mathbf{D}\,\mathbf{Q}^T$ where $\mathbf{D}$ is the diagonal matrix forming the eigenvalues $\lambda_1, \ldots, \lambda_{n-2}$, and $\mathbf{Q}$ is the matrix formed by orthogonal eigenvectors of $\mathbf{M}^\omega_{offd}$. Then, $\mathbf{M}_r^\omega = \mathbf{Q}\,\mathbf{S}\,\mathbf{Q}^T$ is obtained where $\mathbf{S} = R\,\mathbf{I}_\mathrm{U} + \jmath\,\omega\,\mathbf{D}$. After algebraic manipulations, (7) becomes as follows,

$$P_r \,/\, P_t = |\Upsilon_{n,1} - \Lambda_{2,3}|^2 \,/\, 2\,\mathrm{Re}\{\zeta_1\,\zeta_2\} \quad (8)$$

where $\Lambda_{i,j} = \mathbf{M}_i \left(\mathbf{M}_r^{\omega_0}\right)^{-1} \mathbf{M}_j^T$, $\Upsilon_{i,j} = \jmath\,\omega_0 M_{i,j}$, $\mathbf{M}_2 = \left[\begin{array}{ccc} \Upsilon_{2,n} & \Upsilon_{3,n} & \cdots \Upsilon_{n-1,n} \end{array}\right]$, $\mathbf{M}_3 = \left[\begin{array}{ccc} \Upsilon_{1,2} & \Upsilon_{1,3} & \cdots \Upsilon_{1,n-1} \end{array}\right]$, $\zeta_1 = R + Z_L^{\omega_0} - \Lambda_{2,2}$, $\zeta_2 = (R - \Lambda_{3,3})^*$ and

$$Z_L^{\omega_0} = \frac{\left(\det|\mathbf{M}_{n,n}^{\omega_0}|\right)^*}{\left(\det|\mathbf{M}_{n-1,n-1}^{\omega_0}|\right)^*} = \Big(R - \Upsilon_{1,n}\frac{(\Upsilon_{1,n} - \Lambda_{2,3})}{(R - \Lambda_{3,3})} + \left(\left(\Upsilon_{1,n}\mathbf{M}_3 - R\,\mathbf{M}_2\right)/R\right)\left(\mathbf{M}_r^{\omega_0} - \mathbf{M}_3^T\,\mathbf{M}_3/R\right)^{-1}\mathbf{M}_2^T\Big)^* \quad (9)$$

Using $\mathbf{M}_r^{\omega} = \mathbf{Q}\,\mathbf{S}\,\mathbf{Q}^T$ and (9), $\mathrm{Re}\{\zeta_1\,\zeta_2\}$ becomes as follows,

$$\mathrm{Re}\{\zeta_1\,\zeta_2\} = 2R^2\left(1 + \chi_4 + \chi_5 + \chi_4\,\chi_5 - \chi_1^2/2\right) + \omega_0^2\left(M_{1,n}^2 - M_{1,n}\,\chi_3 + \chi_3^2\right) + M_{1,n}\,\chi_2 \quad (10)$$

where $\mathbf{M}_{k,Q} = \mathbf{M}_k\,\mathbf{Q}/(\jmath\,\omega_0)$ for $k = 2, 3$, $\chi_j = \sum_{i=1}^{n-2} Y_j(i)/(R^2/\omega_0^2 + \lambda_i^2)$ for $j \in (1, 5)$ and $Y_1(i) = \mathbf{M}_{2,Q}(i)\,\mathbf{M}_{3,Q}(i)$, $Y_2(i) = \mathbf{M}_{2,Q}^2(i)\,\lambda_i$, $Y_3(i) = Y_1(i)\,\lambda_i$, $Y_4(i) = \mathbf{M}_{2,Q}^2(i)$, $Y_5(i) = \mathbf{M}_{3,Q}^2(i)$. On the other hand, the numerator of (8) is expressed as the following,

$$|\Upsilon_{n,1} - \Lambda_{2,3}|^2 = \omega_0^2 M_{n,1}^2 - 2\omega_0^2 M_{n,1}\chi_3 + R^2\chi_1^2 + \omega_0^2\chi_3^2 \quad (11)$$

In simulations, performed with capacitance between 10-50 pF, r_w of 0.4060 to 0.7250 mm, r between 1-30 m, l between 20-400 m and for $N \times N \times N$ grid network of $N = 3, 4$ or 5, only some components of (10) and (11) dominate. (10) is approximated as either $2R^2$ or $2R^2(1 + \chi_4 + \chi_5 + \chi_4\,\chi_5)$ and (11) is approximated as either $R^2\chi_1^2$ or $R^2\chi_1^2 + \omega_0^2\chi_3^2$. Furthermore, it is observed that $\mathbf{M}_{2,Q}$, $\mathbf{M}_{3,Q}$ and λ_i are proportional to $\propto r^4/l^3$, e.g., $\mathbf{M}_{2,Q}(i) \approx \mathbf{M}_{2,Q}^0(i)\,(r^4/l^3)(l_0^3/r_0^4)$ where $\mathbf{M}_{2,Q}^0$ is the exact value for radius r_0 and the inter-coil distance l_0. Then, by using the approximations for $\mathbf{M}_{2,Q}$, $\mathbf{M}_{3,Q}$, λ_i, (10), (11) and inserting L and R expressions and $R_0 = \rho/\pi\,r_w^2$ into (8), two different approximations for the power loss are given as approximation type-1, i.e.,

$$\frac{P_r}{P_t} \approx \frac{\chi_1^2}{4} + \frac{\omega_0^2\,\chi_3^2}{4\,R^2} = \left(\sum_{i=1}^{n-2}\frac{\mathbf{M}_{2,Q}^0(i)\,\mathbf{M}_{3,Q}^0(i)}{2\,\eta^2 + 2\,(\lambda_i^0)^2}\right)^2 + \left(\sum_{i=1}^{n-2}\frac{\mathbf{M}_{2,Q}^0(i)\,\mathbf{M}_{3,Q}^0(i)\,\lambda_i^0}{\eta\,(2\,\eta^2 + 2\,(\lambda_i^0)^2)}\right)^2 \quad (12)$$

where $\eta = \left(\sqrt{2\,\mu\,\pi}\,n^2\,l^3\,\rho\,C^{1/2}\,r_0^4\right)/\left(r^{5/2}\,r_w^2\,l_0^3\right)$ and approximation type-2, i.e., $P_r/P_t \approx \left(R^2\,\chi_1^2 + \omega_0^2\,\chi_3^2\right)\left(4\,R^2\,(1 + \chi_4\,\chi_5)\right)$. It is found that the approximation type-1 gives accurate results for $r \leq l$ which is the case for practical networks. Since the mutual inductance and therefore $\mathbf{M}_{2,Q}$, $\mathbf{M}_{2,Q}$ and λ_i depend on n_t as square power, the dependence of η on n_t^2 is canceled out leaving the power loss independent of n_t. The other parameter dependencies are extracted by examining η such that the parameters are ordered from the most to least significant factor as l, r, r_w and C. The power loss increases as the radius or wire diameter decreases, capacitance or the inter-coil distance increases. This result is valid for symmetric grid networks, however, for other topologies, different proportionality ratios can be found by analyzing (8).

IV. Conclusion

Underwater MI wireless communication networks using induction coils are presented as promising candidates for underwater communication. SNR performance of 3D underwater networking topologies are theoretically modeled. 3D grid topologies are introduced for shallow and deep water, small and large area coverage networks. Furthermore, SNR, BER, connectivity and bandwidth performances of the proposed networks are numerically analyzed showing that between a few and tens of KHz wireless communication is possible with significantly high SNR for networking areas reaching to a few km^2 in deep sea by forming a fully connected and power efficient multi-coil network. Moreover, the performance dependence of the grid network on inter-coil distance, coil radius, wire diameter and the capacitance is explored theoretically. The analysis of different underwater networking topologies, the effects of moving coils, multiple-access and broadcast mechanisms can be analyzed for future works.

References

[1] I. F. Akyildiz, D. Pompili, and T. Melodia, "Underwater acoustic sensor networks: Research challenges," *Ad Hoc Networks*, vol. 3, no. 3, pp. 257–279, 2005.

[2] J.-H. Cui, J. Kong, M. Gerla, and S. Zhou, "Challenges: building scalable mobile underwater wireless sensor networks for aquatic applications," *IEEE Network*, vol. 20, no. 3, pp. 12–18, 2006.

[3] X. Che, I. Wells, P. Kear, G. Dickers, X. Gong, and M. Rhodes, "A static multi-hop underwater wireless sensor network using RF electromagnetic communications," in *Proc. 2009 IEEE Int. Conf. on Distributed Computing Systems Workshops*, pp. 460–463.

[4] M. Stojanovic, "Underwater wireless communications: Current achievements and research challenges," *IEEE Oceanic Engineering Society Newsletter*, vol. 41, no. 2, 2006.

[5] L. Butler, "Underwater radio communication," *Amateur Radio*, Apr. 1987.

[6] I. Vasilescu, K. Kotay, D. Rus, M. Dunbabin, and P. Corke, "Data collection, storage, and retrieval with an underwater sensor network," in *Proc. 2005 ACM Int. Conf. on Embedded Networked Sensor Systems*, pp. 154–165.

[7] Z. Sun and I. Akyildiz, "Magnetic induction communications for wireless underground sensor networks," *IEEE Trans. Antennas Propag.*, vol. 58, no. 7, pp. 2426–2435, 2010.

[8] D. Anguita, D. Brizzolara, and G. Parodi, "Building an underwater wireless sensor network based on optical communication: research challenges and current results," in *Proc. 2009 IEEE Int. Conf. on Sensor Technologies and Applications*, pp. 476–479.

[9] M. Stojanovic and J. Preisig, "Underwater acoustic communication channels: propagation models and statistical characterization," *IEEE Commun. Mag.*, vol. 47, no. 1, pp. 84–89, 2009.

[10] Z. Sun and I. Akyildiz, "Underground wireless communication using magnetic induction," in *Proc. 2009 IEEE International Conference on Communications*, pp. 1–5.

[11] J. Wang, "A novel magnetic communication system for wireless transmission operating at 14.9 MHz," in *Proc. 2007 IEEE Radio and Wireless Symposium*, pp. 59–62.

[12] R. Bansal, "Near-field magnetic communication," *IEEE Antennas Propag. Mag.*, vol. 46, no. 2, pp. 114–115, 2004.

[13] E. Shamonina, V. Kalinin, K. Ringhofer, and L. Solymar, "Magneto-inductive waveguide," *Electron. Lett.*, vol. 38, pp. 371, 2002.

[14] E.Shamonina, V. Kalinin, K. Ringhofer, and L. Solymar, "Magnetoinductive waves in one, two, and three dimensions," *J. Applied Physics*, vol. 92, pp. 6252, 2002.

[15] R. Syms, E. Shamonina, and L. Solymar, "Magneto-inductive waveguide devices, *IEE Proc.-Microwaves, Antennas and Propagation*, vol. 153, no. 2, pp. 111–121, 2006.

[16] R.Syms, O. Sydoruk, E. Shamonina, and L. Solymar, "Higher order interactions in magneto-inductive waveguides," *Metamaterials*, vol. 1, no. 1, pp. 44–51, 2007.

[17] S. Meybodi, J. Nielsen, J. Bendtsen, and M. Dohler, "Magneto-inductive underground communications in a district heating system," in *Proc. 2011 IEEE Int. Conf. on Communications*, pp. 1–5.

[18] Z. Sun and I. Akyildiz, "Deployment algorithms for wireless underground sensor networks using magnetic induction," in *Proc. 2010 IEEE Global Telecommunications Conf.*, pp. 1–5.
[19] Z. Sun, P. Wang, M. Vuran, M. Al-Rodhaan, A. Al-Dhelaan, and I. Akyildiz, "MISE-PIPE: magnetic induction-based wireless sensor networks for underground pipeline monitoring," *Ad Hoc Networks*, vol. 9, no. 3, pp. 218–227, 2011.
[20] J. Agbinya and M. Masihpour, "Excitation methods for magneto inductive waveguide communication systems," in *Proc. 2010 IEEE Broadband and Biomedical Communications*, pp. 1–6.
[21] J. Sojdehei, P. Wrathall, and D. Dinn, "Magneto-inductive (MI) communications," in *Proc. MTS/IEEE Oceans Conf.*, vol. 1, pp. 513–519, 2001.
[22] R. Woodall, F. Garcia, and J. Sojdehei, "Magneto-inductive submarine communications system and buoy," U.S. Patent 6 058 071, May 2, 2000.
[23] M. Rhodes, B. Hyland, and D. Wolfe, "Underwater communications system," Int. Patent WO/2008/015439 , Feb. 7, 2008.
[24] N. Jack and K. Shenai, "Methods and systems for wireless communication by magnetic induction," U.S. Patent App. 11/763961, June 15, 2007.
[25] S. Kim, Y. Won, Y. Lim, K. Seo, and S. Lim, "Design of physical layer for magnetic field area network," in *Proc. 2009 IEEE Int. Conf. on Ubiquitous Information Technologies and Applications*, pp. 1–4.
[26] J. Agbinya and M. Masihpour, "Power equations and capacity performance of magnetic induction body area network nodes," in *Proc. 2010 IEEE Broadband and Biomedical Communications*, pp. 1–6.
[27] Y. Tak, J. Park, and S. Nam, "Mode-based estimation of 3 db bandwidth for near-field communication systems," *IEEE Trans. Antennas Propag.*, vol. 59, no. 8, pp. 3131–3135, 2011.
[28] J. Casanova, Z. Low, J. Lin, and R. Tseng, "Transmitting coil achieving uniform magnetic field distribution for planar wireless power transfer system," in *Proc. 2009 IEEE Radio and Wireless Symposium*, pp. 530–533.
[29] Y. Won, S. Kang, K. Hwang, S. Kim, and S. Lim, "Research for wireless energy transmission in a magnetic field communication system," in *Proc. 2010 IEEE Int. Symp. on Wireless Pervasive Computing*, pp. 256–260.
[30] I. Yoon and H. Ling, "Investigation of near-field wireless power transfer under multiple transmitters," *IEEE Antennas Wireless Propag. Lett.*, vol. 10, no. 99, pp. 662–665, 2011.
[31] B. Cannon, J. Hoburg, D. Stancil, and S. Goldstein, "Magnetic resonant coupling as a potential means for wireless power transfer to multiple small receivers," *IEEE Trans. Power Electron.*, vol. 24, no. 7, pp. 1819–1825, 2009.
[32] S. Tumanski, "Review article: induction coil sensors—a review," *Measurement Science and Technol.*, vol. 18, pp. R31–R46, 2007.
[33] S. Babic, F. Sirois, and C. Akyel, "Validity check of mutual inductance formulas for circular filaments with lateral and angular misalignments," *Progress in Electromagnetics Research M (PIER M)*, vol. 8, pp. 15–26, 2009.
[34] C. Schilstra and J. Van Hateren, "Using miniature sensor coils for simultaneous measurement of orientation and position of small, fast-moving animals," *J. Neurosci. Methods*, vol. 83, no. 2, pp. 125–131, 1998.
[35] Z. Popovic and B. D. Popovic, *Introductory Electromagnetics*. Prentice Hall, 2000.
[36] J. Claycomb, N. Tralshawala, and J. Miller Jr., "Theoretical investigation of eddy-current induction for nondestructive evaluation by superconducting quantum interference devices," *IEEE Trans. Magn.*, vol. 36, no. 1, pp. 292–298, 2000.
[37] D. Cheng, *Field and Wave Electromagnetics*. Addison-Wesley, 1983.
[38] K. Ocegueda and A. Rodriguez, "A simple method to calculate the signal-to-noise ratio of a circular-shaped coil for MRI," *Concepts in Magnetic Resonance Part A*, vol. 28, no. 6, pp. 422–429, 2006.
[39] J. Proakis and M. Salehi, *Digital Communications*. McGraw-Hill, 1995.
[40] G. Strang, *Introduction to Linear Algebra*. Wellesley Cambridge, 2003.
[41] SoundLink Underwater Acoustic Modems, LinkQuest Inc., USA, 2011. Available: http://www.link-quest.com/
[42] High-Bandwidth Underwater Transceiver, Ambalux Corp., USA, 2012. Available: http://www.ambalux.com
[43] F. Hanson and S. Radic, "High bandwidth underwater optical communication," *Applied Optics*, vol. 47, no. 2, pp. 277–283, 2008.
[44] A. Palmeiro, M. Martin, I. Crowther, and M. Rhodes, "Underwater radio frequency communications," in *Proc. 2011 IEEE Oceans*, pp. 1–8.
[45] Seatooth S300: Through-water Radio Modem, WFS Defense Inc., USA, 2012. Available: http://www.wfs-tech.com

Burhan Gulbahar received the B.Sc. and M.Sc. degrees in electrical and electronics engineering from Bilkent University, Ankara, Turkey, in 1999 and 2002, respectively. He had been a research assistant at Next-generation and Wireless Communications Laboratory (NWCL) and has received his Ph.D. degree in electrical and electronics engineering from Koc University, Istanbul, Turkey in January 2012. His current research interests are in nanoscale optical communications, graphene and carbon nanotube communication networks, underwater communications, cognitive radio networks, wireless communications and quantum communications.

Ozgur B. Akan (M'00-SM'07) received the Ph.D. degree in electrical and computer engineering from the Broadband and Wireless Networking Laboratory, School of Electrical and Computer Engineering, Georgia Institute of Technology, Atlanta, in 2004. He is currently Associate Professor with the Department of Electrical and Electronics Engineering, Koc University and the Director of Next-generation and Wireless Communications Laboratory (NWCL). His current research interests are in wireless communications, bio-inspired communications, nano-scale and molecular communications, network information theory.

Dr. Akan is an Associate Editor for IEEE TRANSACTIONS ON VEHICULAR TECHNOLOGY, *International Journal of Communication Systems* (Wiley), *Nano Communication Networks Journal* (Elsevier), *European Transactions on Telecommunications*. He served as an Editor for *ACM Wireless Networks Journal* (2004-2010), *AD HOC Networks Journal* (Elsevier) (2004-2008), as a Guest Editor for several special issues, as the General Co-Chair for ACM MobiCom 2012, General Chair for IEEE MoNaCom 2012, TPC Co-Chair for IEEE ISCC 2012, TPC Co-Chair for the ACM MSWiM 2010, International Vice Chair for IEEE INFOCOM 2006, and in organizing committees and TPC of many conferences.

He is an IEEE Communications Society Distinguished Lecturer (2011-2012), IEEE Senior Member (Communications Society), and a member of ACM. He is the Vice President for IEEE Communications Society - Turkey Section. Dr. Akan received the IEEE Communications Society Outstanding Young Researcher Award 2010 for EMEA Region (as runner-up), the IBM SUR Award 2011, the IBM Faculty Award twice in 2010 and 2008, Turkish Academy of Sciences Distinguished Young Scientist Award 2008 (TUBA-GEBIP).